Predictive modelling and adaptive long-term performance optimization of an HT-PEM fuel cell based micro combined heat and power (CHP) plant

Alireza Haghighat Mamaghani, Behzad Najafi *, Andrea Casalegno, Fabio Rinaldi

Dipartimento di Energia, Politecnico di Milano, Via Lambruschini 4, 20156 Milano, Italy

In fuel cell based combined heat and power (CHP) plants, degradation within the fuel cell stack and the steam methane reformer significantly affects the generated electrical and thermal power. As a conse-quence, incorporating system's degradation within the model of the plant could be of great importance in order to estimate the resulting variations in the electrical and thermal power generation and taking appropriate measures to mitigate such deviations. To this end, in the present article, a multi-objective optimization approach has been proposed and employed to find the optimal operating parameters of an HT-PEM fuel cell based micro-CHP system within the first 15,000 h of operation while considering the impact of degradation. Two different optimization procedures with the following objective functions have been applied: (I) net electrical efficiency and thermal generation; and (II) net electrical efficiency and electrical power generation. Steam to carbon ratio, auxiliary to process fuel ratio, fuel partialization level and anodic stoichiometric ratio are the design parameters. Based on the results of optimization pro-cedure I, the highest achievable net electrical efficiency at the beginning of operation is 32.75% which, due to degradation, considerably declines to 29.51% in the last time interval. Moreover, in all time steps, optimal solutions cover a wide domain of thermal generation which assures the capability of the system to easily cope with the thermal demand of the user. On the other hand, optimization procedure II displays a steady decrease in both electrical efficiency and electrical generation through time which indicates the adverse effect of degradation on these two performance indices. Finally, it has been found that, using optimization procedure I, the cumulative average electrical efficiency of the plant improved from 26.03% at normal operation to 27.56% at optimized condition. Furthermore, it was determined that by employing the optimal points obtained in optimization procedure II, the average cumulative electrical power generation is increased from 25.4 kW (at normal operation) to 26.8 kW. It is noteworthy that, the study not only provides some insights into the long-term performance of such system, but can be more importantly perceived as a guideline to adaptively optimize the operating conditions of the system in order to alleviate the degradation's effect and to guarantee optimal performance of the system throughout its lifetime.

Keywords: Combined heat and power, High temperature PEM fuel cell, Degradation, Long-term performance, Adaptive optimization, Multi objective optimization

HIGHLIGHTS

- Adaptive long-term performance optimization of an HT-PEM fuel cell based CHP plant is studied.
- The impact of degradation, within the fuel cell and reformer, on the system's performance is considered.
- At each interval, a set of optimal points each of which is a trade-off between the objectives is obtained.
- Electrical and thermal generation and the net electrical efficiency were selected as objective functions.
- Performance of the system operated at normal condition vs optimized condition was compared.

1. Introduction

In the past decade, scarcity of primary energy sources and stringent environmental legislations concerning the emissions of

Article history:
Received 15 April 2016
Received in revised form 29 July 2016
Accepted 8 August 2016
Available online xxxx

* Corresponding author.
E-mail addresses: alireza.haghighat@mail.polimi.it (A. Haghighat Mamaghani), behzad.najafi@polimi.it (B. Najafi), andrea.casalegno@polimi.it (A. Casalegno), fabio.rinaldi@polimi.it (F. Rinaldi)..

© 2016. This manuscript version is made available under the CC-BY-NC-ND 4.0 license http://creativecommons.org/licenses/by-nc-nd/4.0/
Published Journal Article available at http://dx.doi.org/10.1016/j.apenergy.2016.08.050

Nomenclature

Acronyms

aux/proc	auxiliary to process flow rate ratio
CHP	combined heat and power
GDL	gas diffusion layer
HT-PEM	high temperature proton exchange membrane
MEA	membrane electrode assembly
OHM	ohmic
PBI	polybenzimidazole
S/C	steam to carbon ratio
SMR	steam methane reforming
WGS	water gas shift
WKO	water knock out

Symbols

E_{ID}	ideal voltage (V)
E_a	activation energy (kJ/mol)
f	friction factor
ΔH_{298K}	standard enthalpy of reaction (kJ kmol^{-1})
I	current (A)
k	rate coefficient
K	equilibrium constant
LHV	low heating value (kJ kg^{-1})
$\dot{m}$	mass flow rate (kg s^{-1})
N	number of cells
P	power (kW)
r	rate of reaction (mol lit^{-1} s^{-1})
R	universal gas constant (kJ kmol^{-1} K^{-1})
T	temperature (K)
V	voltage (V)

Subscripts

A	anode
B	burner
C	cathode
el	electrical

Greek symbols

η_A	anodic voltage loss
η_C	cathodic voltage loss
η_{el}	electrical efficiency
λ_{H_2}	anodic stoichiometric ratio

contaminants have set the focus on developing new technologies for more environmentally benign and more efficient power production systems [1,2]. One of the most acknowledged approaches in combating the aforementioned challenges is the usage of fuel cell technology in order to cater the electricity and heat demand of domestic dwellings which is responsible for a large part of total energy consumption in Europe [3]. Among different available technologies, fuel cells can be taken into account as one of the most encouraging options for future low-energy building concept. Fuel cell based micro-combined heat and power (micro-CHP) systems can reach higher electrical efficiencies in comparison with micro-CHPs based on heat engines while they also offer lower heat-to-power ratio.

Proton exchange membrane (PEM) fuel cell is amongst the most developed technologies for CHP applications and it covers around 90% of the fuel cell based CHP plants [4]. In this regard, many works have been dedicated to modelling and simulation, performance evaluation, and optimization of fuel cell based CHP plants [5–7]. Guizzi and Manno [8] carried out energetic and economic analyses on a cogeneration system based on a PEM fuel cell which was able to achieve net electrical and thermal efficiency of 41.93% and 64.16% respectively at rated conditions. In another study, Jannelli et al. [9] compared the performance of three cogeneration systems based on LT-PEM and HT-PEM fuel cells. The results showed that systems based on the HT-PEM fuel cell achieve electrical efficiency and first law efficiency up to 40% and 79% respectively. Zuliani and Taccani [10] analyzed the performance of a 1 kW HT-PEM based cogeneration system and reported that at design load, the system can reach electrical efficiency of 26% and the total efficiency of 78% while offering a simpler balance of plant compared to a LT-PEM based system. Kang et al. [11] applied a model of a 20 kW PEM fuel cell based system in ASPEN HYSYS to investigate the impacts of main operating parameters on the electrical and thermal efficiency of the plant. The simulation data reveal that the fuel delivery rate and air-fuel ratio supplied into the burner are crucial factors to obtain the desired electrical power and an acceptable CO concentration level. In another research, Napoli et al. [12] performed a techno-economic analysis on PEMFC and SOFC based micro CHP systems and concluded that for both cases, the investment cost is the main obstacle to compete with the conventional technologies. A thermo-economic analysis on an HT-PEM fuel cell based CHP systems showed that the average per-unit cost (PUC) of electrical power is 15–19,000/kWe, while the average PUC of electrical and heat recovery power is 7000–9000/kW [13]. Herdem et al. [14] carried out a parametric study on a methanol reformate gas fuelled HT-PEM fuel cell based system and demonstrated that the effect of CO molar ratio on the fuel cell performance declines with fuel cell temperature. The fuel cell voltage diminishes around 78% with an increment in current density from 0.1 A/cm^2 to 1 A/cm^2 for 160 °C fuel cell temperature and 0.9% CO molar ratio in the reformate gas. One of the approaches to increase the net electrical efficiency of the system is to harness the generated heat within the plant via organic Rankine cycle (ORC) and convert it to electrical power [15]. For this purpose, Perna et al. [16] integrated an HT-PEM fuel cell system with an ORC unit and compared the performance of the plant with and without the ORC unit. The obtained results revealed that the integration with an ORC unit can significantly boost the electrical production by 10%. Wu et al. [17] studied the performance of a polybenzimidazole (PBI) based HT-PEM fuel cell stack under air-breathing conditions. Their results suggested that a peak power density of 220.5 mW cm^{-2} at 200 °C can be achieved without employing any water management, which is comparable to those achieved with LT-PEM units.

Almost all fuel cell technologies suffer from degradation over time which results in performance deterioration and extra cost for replacement or repairing of the components. This issue is of particular importance and has been widely underscored in the case of fuel cell based CHP plants given the severe degradation in fuel cell stack. As a consequence, a number of studies have been focused on novel approaches for modelling the degradation and optimizing the operating conditions of the stack to alleviate the negative effect of degradation and elongate the system's lifetime. Pohl et al. [18] proposed a novel method for modelling the degradation within HT-PEM fuel cells using dual time scale simulations with shorter simulation time by approximately 73% compared to conventional simulation approaches. In another research, Zhang et al. [19] conducted an optimization on the operating temperature of HT-PEM fuel cell and based on their experimental results, the optimal operating temperature window is between 160 °C and 180 °C by compromising among the cell performance, CO tolerance

and durability. Similarly, Kim et al. [20] developed experimentally validated models to predict the durability of HT-PEM fuel cell at different operating temperatures. Galbiati et al. [21] performed an experiment on degradation of an HT-PEM fuel cell with PBI-based membrane and suggested that increasing the temperature from 160 °C to 180 °C results a growth in degradation from 8 $\mu V\,h^{-1}$ to 19 $\mu V\,h^{-1}$. Given the aforementioned facts, in order to provide a realistic understanding of the system in long-term and a solid basis for economic plans, degradation throughout the lifetime of the system should be integrated in the CHP system analysis. Mocoteguy et al. [22] studied the long-term operation of an HT-PEM based micro-CHP and showed that in the first 500 h of operation stack's performance varies slightly while after 658 h of operation the electrical efficiency dropped from 30.6% to 28.3%. In another research work, Hawkes et al. [23] developed a mathematical model for techno-economic analysis of fuel cell micro-CHP system while taking into account the stack degradation.

Due to the high investment cost of fuel cell based energy systems, in order to maximize the profit, optimizing the operation of the plant from energetic point of view is of great importance. Accordingly, a number of researches have been focused on optimization of fuel cell based systems. Di Marcoberardino et al. [24] studied the integration of an autothermal membrane reformer with a 5 kW PEM fuel cell based micro-CHP system. In their study, optimization of the plant based on thermodynamic objectives (net electric efficiency and total system efficiency) was performed with different configuration and operating conditions. Gandiglio et al. [25] designed and optimized an LT-PEM based CHP system for residential applications. Their results showed that the maximum achieved electrical efficiency is around 36% (AC, LHV) and the considered micro-CHP PEM system is able to supply around 22.4% of the heat demand of a 50 m^2 medium-low efficiency building. In another research, Barelli et al. [26] developed a model of a PEM fuel cell CHP system in Aspen Plus environment to assess energetic and exergetic efficiency of the system and locate the optimal operating conditions. In another work, Godat and Marechal [27] studied the optimization of an LT-PEM fuel cell to find the optimal operating conditions and process structure of the system using process integration techniques. The electrical efficiency of the system was increased from 35% for the reference system to 49% in the optimized design. Arsalis et al. [28] optimized an HT-PEM FC based micro-CHP system which caters the residential needs for heating and electricity in detached single-family households in Denmark. Their results demonstrated an average net electrical efficiency and average total system efficiency of 0.380 and 0.815 respectively.

The principal goal of this article is to assess the optimum long-term performance of an HT-PEM fuel cell based micro CHP plant by applying two different multi-objective optimization approaches. In the first optimization method, net electrical efficiency and thermal generation have been selected as objectives functions while in the second one thermal generation was replaced by electrical generation. Steam to carbon ratio, auxiliary to process fuel ratio, fuel partialization level and anodic stoichiometric ratio have been chosen as design parameters. In both optimization approaches, for each time interval, the result of optimization is a Pareto frontier which is a set of optimal points each of which is a trade-off between the desired objective functions. The ultimate purpose of combining multi-objective optimization and degradation prediction is to provide sets of operating parameters which are capable of covering a wide range of thermal/electrical power generation and also offering the maximum achievable electrical efficiency during system's operation. Finally, in order to emphasize the advantage of employing multi-objective optimization, values of lifetime electrical efficiency and electrical generation at two different operating conditions, normal and optimized, have been compared. It is worth mentioning that, the results obtained in the study provides a guideline for progressive modification of operating conditions in order to mitigate the degradation effects and to maximize the long-term performance of the plant.

2. Plant description

The configuration of the HT-PEM fuel cell based micro CHP plant can be seen in Fig. 1. Three main pathways or flow streams can be considered in the system including: syngas flow which is showed by red[1] color and starts from the SMR reactor and eventually enters the anodic side of the fuel cell; low pressure water circuit with light blue color which absorbs heat from the cathodic outlet stream and flue gases leaving the plant; and high pressure water circuit with navy blue color which captures heat in heat exchangers before the water gas shift reactor, after the anodic recuperator and superheater and finally provides superheated steam for reforming reactions within the SMR. Before entering the ejector, natural gas is first desulfurized due to the low resistance of PEM fuel cell to sulfur compounds. Afterwards, the desulfurized natural gas is mixed with superheated steam and the mixture undergoes the reforming reactions in the SMR and the hydrogen rich reformate is produced. A part of the fed natural gas is considered as auxiliary fuel and injected into the burner and the resulting high temperature combustion gases are utilized to provide the required heat for endothermic reforming reactions in the SMR. It should be mentioned that the amount of the fuel to the burner and the air to fuel ratio can be regulated to have a specific combustion gas temperature. The produced syngas in SMR is then entered the WGS where the CO concentration is brought down to acceptable levels imposed by the properties of the PEM fuel cell. Prior to the fuel cell and due to the limitation of PEM fuel cell regarding water management, the water content of syngas is reduced using a heat exchanger and a water knock-out (WKO). In the fuel cell stack, hydrogen and oxygen react according to the electrochemical reactions and generate electricity, waste heat and water. The waste heat generated by the electrochemical reactions is provided to Thermal User 1 by means of an oil circulation system. On the other hand, thermal energy collected from different parts of the plant by the low pressure water circuit goes to Thermal User 2.

3. Model description

3.1. Fuel processor

3.1.1. steam methane reformer

In the present study, a steam methane reformer (SMR) has been utilized to provide the required hydrogen for electrochemical reaction. In order to model the SMR unit, a 1D steady state and non-isothermal plug flow reactor with shell and tube heat exchanger configuration has been modelled in the MATLAB environment. It should be pointed out that in the developed SMR model, due to the small diameter of the tube side of the reformer (where reactions take place) concentration and temperature gradients in the radial direction are considered to be insignificant and also it is assumed that the rate determining step is the surface catalytic reaction. The kinetic model of steam methane reforming proposed by Xu and Froment [29] has been employed to model the reaction kinetics. The developed model is next validated using experimental data obtained from a setup with the same geometry designed and implemented by our industrial partner, ICI Caldaie S.p.A. Through the model development, two separate working media have been simulated: the tube side, filled with catalyst, in which the reactions occur and the shell side where the combustion gases from the

[1] For interpretation of color in Figs. 1 and 5, the reader is referred to the web version of this article.

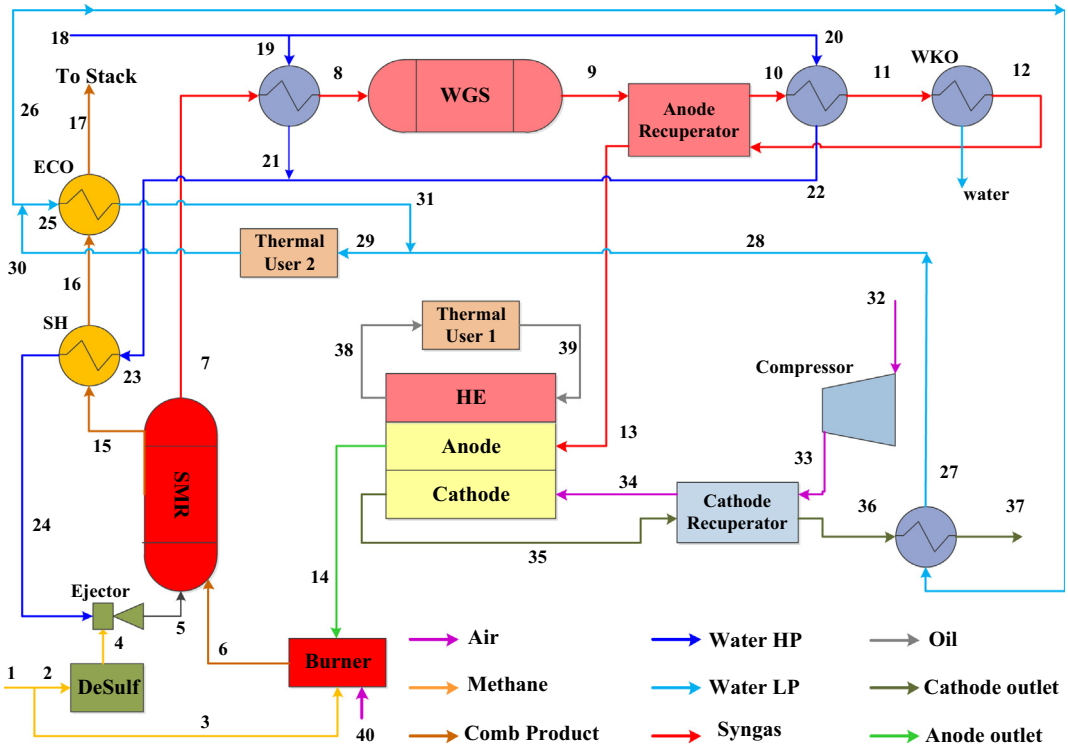

Fig. 1. Schematic view of the HT-PEMFC based CHP plant.

burner flow and provide the required heat for endothermic reactions. The catalyst structure and composition owing to the confidentiality of the manufacturer's data are not reported. The main reactions taking place within the steam reformer are listed below:

$$CH_4 + H_2O \Longleftrightarrow CO + 3H_2 \quad \Delta H_{298K} = +206\ kJ/mol \tag{1}$$

$$CO + H_2O \Longleftrightarrow CO_2 + H_2 \quad \Delta H_{298K} = -41\ kJ/mol \tag{2}$$

$$CH_4 + 2H_2O \Longleftrightarrow CO_2 + 4H_2 \quad \Delta H_{298K} = +165\ kJ/mol \tag{3}$$

Xu and Froment [29] proposed a general and realistic Langmuir–Hinshelwood type kinetic model for methane steam reforming considering the water–gas shift reaction to occur in parallel with the steam reforming reactions. The details of kinetic coefficients, and the assumptions considered while developing the model can be found in the previous work of the authors [30,29].

3.1.2. Water gas shift reactor

Employing water gas shift reactor downstream of the SMR brings about two main advantages: on the one hand, the hydrogen yield is enhanced resulting in higher electrical efficiency for the fuel cell, and on the other hand, carbon monoxide content, which adversely affects the fuel cell voltage, is reduced. The kinetics equations proposed by Keiksi et al. [31] for high temperature WGS with Fe_3O_4-Cr_2O_3 as catalyst have been employed. Considering the fact that the WGS reaction is exothermic and favored by low temperature, a heat exchanger located upstream of the WGS reactor reduces the temperature of the syngas to a desired level.

3.2. HT-PEM fuel cell stack

The HT-PEM fuel cell stack is basically made up of three main parts including the pre-heater, the membrane electrode assembly (MEA), and the oil cooling circuit. The reactants (syngas and compressed air) first go through the pre-heater where they exchange heat with the circulating oil to reach the stack temperature. In the MEA, hydrogen and oxygen participate in the electrochemical reaction resulting in heat, water and electricity. The MEA can be divided into three main parts: cathodic and anodic channels, the gas diffusion layer (GDL) and the anodic and cathodic electrodes. The GDL is a pathway for hydrogen and oxygen to access the catalyst layer where the electrochemical reaction occurs. The cathodic and anodic electrodes are separated by a polybenzimidazole membrane. Table 1 represents the main geometric parameters of the fuel cell stack used for the simulation.

The MEA domain is modelled using a quasi 2D approach in which the integration is carried out in two coordinates: along the channel and along the MEA thickness. Hydrogen and oxygen are gradually consumed through the channel owing to the electrochemical reactions while water is consequently produced. In order to determine the species concentration profiles mass conservation is taken into account.

The current density (reaction rate) is determined employing the following equations:

$$V = E_{ID} - \eta_{OHM} - \eta_C - \eta_A \tag{4}$$

$$P_{stack} = V_{cell} I_{stack} N \tag{5}$$

where V is the single cell voltage, E_{ID} is the ideal voltage by Nernst equation, η_{OHM} is the ohmic loss, and η_C and η_A are the cathode and anode activation losses respectively.

Table 1
The geometric parameters of the HT-PEM fuel cell stack.

Geometric parameter	Value
Channel length (cm)	76.25
Channel height (cm)	0.2
Cell width (cm)	7.6
Number of channels	38
Number of cells	440

Table 2
The values of the parameters used for the HT-PEM fuel cell modelling.

Symbol	Value	Description
C_{ref}/mol cm^{-3}	$5.88 \cdot 10^{-6}$	Reference O_2 concentration
δ_{GDL}/cm	0.04	GDL thickness, anode/cathode
δ_{MEM}/cm	0.015	Membrane thickness [36]
ε/τ_{GDL}/-	0.084	Porosity/ tortuosityGDL, anode/cathode
θ_{H2PO4-}/–	0.05	$H_2PO_4^-$ coverage [36]
E_0/V	$1.256–2.4 \cdot 10^{-4}$.T	Ideal potential
α_C/–	0.85	Charge transfer coefficient cathode [32]
E_{ORR}/J mol^{-1}	$102.86 \cdot 10^3$	Activation energy ORR [36]
$i_{0,ORR}$/A cm^{-2}	$3.28 \cdot 10^{-6}$	Exchange current density ORR [36]
α_A/–	0.5	Charge transfer coefficient anode [36]
E_{HOR}/J mol^{-1}	$2.5 \cdot 10^3$	Activation energy HOR
$i_{0,HOR}$/A cm^{-2}	$1.25 \cdot 10^3$	Exchange current density HOR [35]
$E_{COR,\ C}$/J mol^{-1}	$127 \cdot 10^3$	Activation energy COR [35]
$i_{0,COR}$/A cm^{-2}	$2.2 \cdot 10^{13}$	Exchange current density cathode [35]
$E_{ADS,H}$/J mol^{-1}	$10.4 \cdot 10^3$	Activation energy hydrogen adsorption [35]
$k_{ADS,H}$/cm s^{-1}	5.96	Hydrogen adsorption constant [35]
$E_{ADS,CO}$/J mol^{-1}	$47.3 \cdot 10^3$	Activation energy CO adsorption [35]
$k_{ADS,CO}$/cm s^{-1}	$1.5 \cdot 10^5$	CO adsorption constant [36]
$E_{DES,H}$/J mol^{-1}	$98.3 \cdot 10^3$	Activation energy hydrogen desorption [35]
$k_{DES,H}$/cm s^{-1}	$2.5 \cdot 10^3$	Hydrogen desorption constant [35]
$E_{DES,CO}$/J mol^{-1}	$147 \cdot 10^3$	Activation energy CO desorption [35]
$k_{DES,CO}$/cm s^{-1}	$1.03 \cdot 10^3$	CO desorption constant [35]
β_{CO}/–	0.1	Frumkin isotherm symmetry factor [35]
r_{CO}/J mol^{-1} K^{-1}	56.5	Frumkin isotherm lateral interaction parameter [35]
σ_{GDL}/S cm^{-1}	9	GDL conductivity [34]
σ_0/S cm^{-1} K^{-1}	$9.4 \cdot 10^3$	Membrane conductivity parameter[32]
$E_{\sigma,MEM}$/J mol^{-1}	$18.5 \cdot 10^3$	Activation energy membrane conductivity [32]
D_m/cm^2 s^{-1}	0.001	Membrane water permeation coefficient

E_{ID} (ideal voltage) is determined as a function of temperature from the Gibbs free energy formation data. The Ohmic loss is the summation of the resistances of the bipolar plates, GDLs, and the electrolyte and is assumed to follow the Ohm's law. It is also presumed that the electrolyte conductivity follows the Arrhenius law and it is taken from [32]. The electrolyte's Ohmic loss is determined using its proton conductivity:

$$\eta_{ohm} = \frac{i\delta_m}{\sigma_{PBI/H_3PO_4}(T)} \tag{6}$$

where

$$\sigma_{PBI/H_3PO_4}(T) = \frac{\sigma}{T} exp\left(-\frac{E_a}{RT}\right) \tag{7}$$

Furthermore, Stefan-Maxwell phenomenological law [33] is applied to model the mass transport within the GDL. The activation losses of the cathodic electrode are supposed to follow the Tafel Law, first order with respect to oxygen concentration [34]:

$$\eta_C \equiv b \cdot \log\left(\frac{i}{i_*}\right) + b \cdot \log\left(\frac{C_{ref}}{C_{O_2,el}}\right) \tag{8}$$

where i_* is the reference exchange current density which follows an Arrhenius like behavior and b, the Tafel slope, is determined using the following correlation:

$$b = RT/(\alpha_C F) \tag{9}$$

As mentioned previously, carbon monoxide has a negative impact on the performance of the fuel cell. The origin of this issue is the adsorption of carbon monoxide on the anode catalyst active sites and consequently retardation of the electrochemical reactions. Accordingly, the adverse effect of CO poisoning on the cell voltage and the fuel cell's performance has been taken into account in the model of the stack. The hydrogen and carbon monoxide oxidation currents are determined using Butler-Volmer equation [35] as follows:

$$i_{H2} \equiv i_{*,H2} \cdot \vartheta_H \cdot 2\sinh\left(\frac{\eta_A}{b_A}\right) \tag{10}$$

$$i_{CO} \equiv i_{*,CO} \cdot \vartheta_{CO} \cdot 2\sinh\left(\frac{\eta_A}{b_A}\right) \tag{11}$$

$$i = i_{CO} + i_{H_2} \tag{12}$$

Furthermore, the summation of the coverage of all the species must be equal to 1; hence:

$$\vartheta_{FREE} = 1 - \vartheta_H - \vartheta_{CO} - \vartheta_{H_2PO_4^-} \tag{13}$$

where the phosphoric acid's coverage ($\vartheta_{H_2PO_4-}$) is taken from [36]. Moreover, Langmuir adsorption for hydrogen and Frumkin adsorption for carbon monoxide, while considering the equilibrium of adsorption, are employed to calculate the hydrogen and carbon monoxide coverage (ϑ_H and ϑ_{CO}).The values of the parameters used in the developed HT-PEM fuel cell stack model are listed in Table 2.

4. System optimization

4.1. Definition of objective functions

In this study, two different optimization procedures have been followed with the same optimization concept but different sets of objective functions. In the first one (optimization procedure I), thermal power generation of the plant which is the sum of the thermal input to User 1 and 2 is one of the objectives and the net electrical efficiency of the system is the second objective. On the other hand, in the optimization procedure II, electrical power generation and net electrical efficiency have been selected as the objective functions. It should be highlighted that in all the optimization methods the impact of degradation within the fuel cell stack and steam methane reformer has been taken into consideration.

The presented analysis is conducted for the first 15,000 h of operation of the system which is an acceptable lifetime for

HT-PEM fuel cell based micro CHP. After 15,000 h of operation, substantial voltage losses in the fuel cell stack and consequently sharp decline in the performance hinder further usage of the system and necessitate repairing or replacement of some of the components [20,37]. Six unequal time intervals have been considered for the first 15,000 h of operation with shorter intervals for periods with sharper degradation in the fuel cell and reformer. In each time interval, the mean degradation value of that period has been employed to estimate the performance indicators and the obtained results are representatives of the whole period. It is important to note that the inlet fuel flow rate fed to the plant is changing in the optimization process due to the variations of auxiliary to process fuel ratio and fuel partialization level.

The net electrical efficiency applied in the optimization procedure is calculated as follows:

$$\eta_{net,el} = \frac{\dot{P}_{el,net}}{\dot{m}_{CH_4,in} LHV_{CH_4}} \quad (14)$$

where the net power output ($\dot{P}_{el,net}$) is the power produced by the fuel cell stack after subtracting losses and auxiliaries

4.2. Design parameters and constraints

Steam to carbon ratio (S/C), anodic stoichiometric ratio (λ_{H_2}),-fuel auxiliary to process ratio (aux/proc), and fuel partialization level (ratio between the provided fuel flow rate and the supplied fuel rate at full load operation) have been chosen as design parameters. With the purpose of obtaining results which are technically viable, several constraints and ranges have been imposed on the system design parameters during optimization. The design parameters and their ranges of variation along with the corresponding constraints are presented in Table 3. Furthermore, the operating conditions of the CHP plant which have been used in the modelling of the system are brought in Table 4.

4.3. Optimization method

One of the major shortcomings of the works dealing with the optimization of fuel cell based CHP systems is that in most of them only one of the performance indices is aimed to be optimized. However, in order to achieve a meaningful and comprehensive understanding of the capacity of the system under optimized conditions, multi-objective optimization could be a useful and practical tool. Different from single-objective optimization, the outcome of a multi-objective optimization problem is not a single optimum point, but a set of non-dominated solutions (Pareto front) which simultaneously satisfy the objective functions at an acceptable level. Once the Pareto front curve is obtained, based on the specific usage, it can be decided which design set is the most suitable.

Table 3
List of constraints for system optimization and the range of variation of design parameters [37,40].

Constraint	Reason
3.5 < S/C < 5.5	Minimum and maximum values of steam to carbon ratio
1.2 < λ_{H_2} < 1.6	Minimum and maximum values of anodic stoichiometric ratio
0.6 < Partialization < 1	Minimum and maximum values of fuel partialization level
0.12 < aux/proc < 0.22	Minimum and maximum values of auxiliary to process fuel ratio
T_8 < 610 K	Due to exothermic nature of WGS reaction
T_{17} > 340 K	To avoid formation of carbonic acid (H_2CO_3) in exhaust gases

Table 4
The fixed design parameters of the HT-PEMFC based CHP plant.

Operating condition	Value
Ambient temperature	20 (°C)
Ambient pressure	1 (bar)
Pressure of high pressure water circuit	7.8 (bar)
Pressure of low pressure water circuit (bar)	2 (bar)
DC/AC inverter efficiency	96 (%)
Cathodic stoichiometric ratio	2
Current density	0.2 (A cm^{-2})
Cell temperature	160 (°C)
Air compressor isentropic efficiency	82 (%)

Table 5
Genetic algorithm parameters in the optimization process.

Tuning parameters	Value
Population size	300
Maximum number of generation	200
Probability of crossover	90%
Probability of mutation	1%
Selection process	Tournament
Tournament size	2

Among different methods for multi-objective optimization, genetic algorithm (GA) is one of the most applied techniques for optimization of energy systems. In genetic algorithm, a solution vector (chromosome or individual) is used to assess the objective functions values (fitness value) and then new generations of solutions are generated from the previous ones by means of crossover and mutation. In the crossover operation, two chromosomes are combined to form new chromosomes (offsprings). Individuals with higher fitness have more chance for being selected and consequently produce offsprings. In the mutation operator, random changes in individuals are employed to aid the population search to escape from local optima by introducing diversity into the population [38,39].

The multi-objective GA implemented in MATLAB optimization toolbox has been employed in the present work and the chosen values for the GA parameters are listed in Table 5.

5. Results and discussion

5.1. Reformer, water gas shift reactor, and HT-PEM stack model validation

In order to validate the developed models of the steam methane reformer and water gas shift reactor, the experimental data obtained from an LT-PEM fuel cell based CHP plant (Sidera30), designed by ICI Caldaie S.p.A are employed. Accordingly, considering the same geometrics and kinetic characteristics of the real plant, while operating at the same operating conditions, the results from the model have been compared with the available experimental data. The analyzed parameters through the validation process include the syngas composition at the outlet of the reformer and the WGS reactor, the temperature of the syngas leaving the fuel processor reactors, and the superheater outlet temperature. The details of the validation procedure and developed model's accuracy have been represented in the author's previous study [30].

In order to confirm the accuracy of the HT-PEM fuel cell model, the experimentally validated model developed by Bergmann et al. [36] has been utilized. In this regard, the polarization curves obtained from the model are compared with the ones reported by Bergmann et al. [36] at different CO concentrations and stack

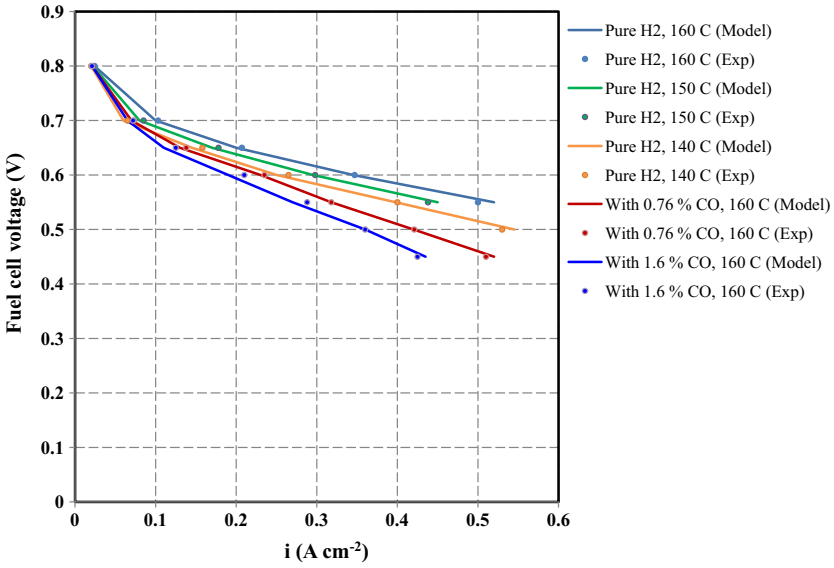

Fig. 2. Validation of the HT-PEM fuel cell stack model.

temperatures. As can be seen in Fig. 2, an acceptable level of accuracy has been achieved by the developed model for simulating the behavior of the HT-PEM fuel cell.

5.2. Degradation model of HT-PEM fuel cell and steam reformer

As mentioned in previous sections, HT-PEM fuel cell suffers from drastic degradation and performance diminution through time. Co-authors of the present article have conducted a comprehensive experimental investigation on the influence of key fuel cell's parameters including stack temperature, current density, and cathodic stoichiometry on the degradation rate of a PBI-based HT-PEM fuel cell [21]. In another research, Kim et al. [20] developed several experimentally validated models to predict the durability and performance trend of an HT-PEM fuel cell under different cell temperatures for long periods of time. Due to the fact that the fuel cell used in the present study and the one employed by Kim et al. [20] have similar characteristics, and given the consistency between the proposed models by Kim et al. [20] and experimental results obtained by co-authors [21], the model reported by Kim et al. is considered to predict the cell voltage drop with time, as depicted in Fig. 3.

Regarding the degradation within the reformer, the experimental data of a long term performance analysis on the steam reformer was provided by the industrial partner, ICI Caldaie S.p.A. Table 6 presents the experimental data on the performance of the reformer for the first 14,000 h of operation.

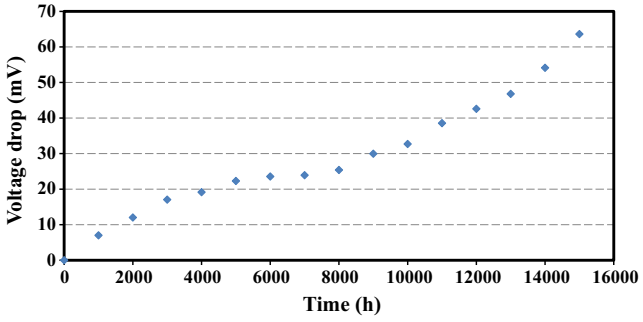

Fig. 3. Voltage drop due to the degradation in time.

5.3. Optimization procedure I

The first optimization procedure is conducted with the aim of investigating the optimal operating conditions of the system while addressing a certain thermal load profile. Accordingly, the thermal generation and the net electrical efficiency are considered as optimization objectives. The optimization procedure has been carried out for a series of time intervals while taking into account the degradation within the system. It is noteworthy that the time steps have been chosen based on the degradation profile of the stack and the steam reformer (see Section 4.1). As can be clearly noticed in Table 6, the steam reformer has a significant degradation at the beginning of operation while, as displayed in Fig. 3, the fuel cell stack experiences substantial voltage loses at the end of the considered lifetime of the plant. As a consequence, the variation in the performance of the system is more significant in the beginning and the end of lifetime and, therefore, shorter time intervals (more time steps) have been selected in these regions.

Fig. 4 demonstrates the obtained Pareto frontier solutions for optimization procedure I at different time intervals. The competing relation between the thermal generation and the net electrical efficiency (i.e. objective functions) can be clearly noticed in the obtained multi-objective optimization curve. Considering the Pareto frontier curve for any time intervals, as the thermal generation increases, the net electrical efficiency significantly deteriorates. Fig. 4 affirms the capability of the system to cover a wide range of thermal generations (from 27 kW to 64 kW) which is a crucial aspect of micro CHP plants for building applications due to the significant thermal load fluctuations. On the other hand, the expected descending trend of the net electrical efficiency with time can be noticed by comparing the maximum achievable electrical efficiency. Taking into account the thermal generation of 28 kW, the net electrical efficiency of 32.75% at the beginning of the operation declines to 29.5% after 14,000 h of operation. The observed reduction in the net electrical efficiency through time could be contributed to two major phenomena: firstly, as mentioned earlier, due to the degradation and considerable voltage losses, the performance of fuel cell diminishes with time which greatly affects the net electrical efficiency. On the other hand, the degradation within

Table 6
Reformer performance in different operating time.

Time (h)	0	2000	4000	6000	8000	10,000	12,000	14,000
Conversion (%)	75.2	72.9	71.3	70.6	69.9	69.4	69.2	69

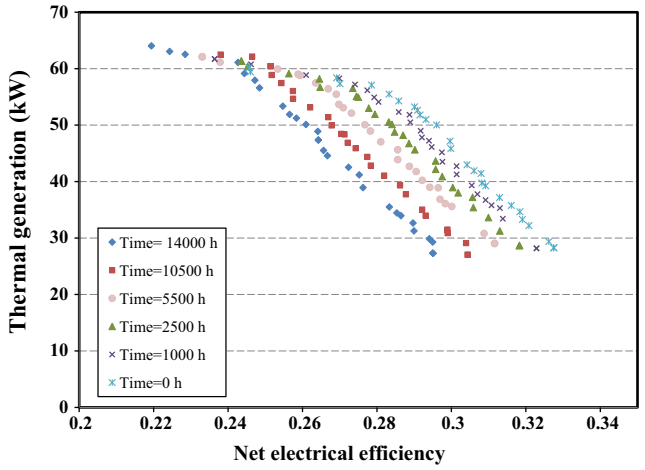

Fig. 4. Pareto front obtained from multi-objective optimization procedure I in different time steps.

the reformer hinders the occurrence of reforming reactions and hydrogen production at reformer's full capacity which, in turn, lowers the amount of hydrogen in the reformate gas entered the anodic side of the fuel cell. The aforementioned issues disable the plant to efficiently utilize natural gas for electricity production and instead amplify the thermal power generation. In order to mitigate the adverse impact of degradation on the net electrical efficiency, amongst the selected design parameters in the optimization process, fuel auxiliary to process ratio and fuel partialization level play key roles. In our previous study [30], it was shown that for steam to carbon ratios smaller than 5, increasing the auxiliary to process fuel ratio in the range of 0.12–0.22 steadily lessens the electrical efficiency. Given the fact that the steam to carbon ratio for all optimal points (Pareto frontier curve), in optimization procure I, is smaller than five, the aforesaid relation between aux/proc and electrical efficiency can be expected in this case. Considering the optimal points at each time interval, a fluctuating but roughly descending trend in aux/proc values with time has been noticed which can be attributed to the fact that employing lower amount of auxiliary fuel boosts the electrical efficiency. Variation in fuel partialization level changes the mass flow rate of the supplied fuel to the plant which can remarkably alter the thermal and electrical generation and subsequently their efficiencies. In this regard, in our previous work [37], we demonstrated that fuel partialization improves the electrical efficiency due to the enhancement in reforming reactions and the decrement in voltage losses in the fuel cell. Monitoring the values of design parameters showed that optimal points on Pareto frontier curves with longer operation times mostly possess smaller values of fuel partialization level which evidences the attempt of the utilized optimization algorithm to nullify the negative effect of degradation on the system's performance. It should be highlighted that higher waste heat in the stack and larger amount of available heat in the superheater and economizer due to the degradation offset the decrement in the thermal generation at lower values of aux/proc and fuel partialization.

In order to further our understanding of the system's behavior, the determined operating conditions and their corresponding net electrical efficiency for optimal points with thermal generation equal to 50 kW at different time steps are compared. The obtained values for design parameters at different intervals are summarized in Table 7. Even though some general predictions can be made regarding the dependence of performance indices on the operating conditions, a significant non-linearity in the trend of obtained optimal parameters can be vividly noticed in Table 7. These non-linear fluctuations in design parameters can explain the necessity of employing a sophisticated stochastic optimization procedure rather than utilizing a conventional parametric study.

Table 7
Optimal operating conditions and the resulting net electrical efficiency at different time steps for 50 kW thermal power generation (optimization procedure I).

Parameter	Time step (h)					
	0	1000	2500	5500	10,500	14,000
Steam to carbon ratio	4.55	4.69	4.66	4.60	4.52	4.58
Auxiliary to process ratio	0.164	0.189	0.147	0.157	0.159	0.141
Anodic stoichiometric ratio	1.211	1.207	1.210	1.204	1.225	1.213
Partialization factor	0.953	0.927	0.955	0.924	0.904	0.912
Net electrical efficiency (%)	29.6	28.8	28.4	27.7	26.8	26.1

Finally, in order to evaluate the ability of the optimization procedure in attenuating the degradation's effect, the achieved electrical efficiency at each time step is compared with the ones obtained during normal operation and partialization strategy (for further information refer to [30]). The data presented in Table 8 clearly-demonstrates that utilizing the obtained optimal points in optimization procedure I can remarkably improves the electrical efficiency of the plant especially at longer lifetimes. For instance, at the beginning of operation, the electrical efficiency of 28.9% at normal operation could be improved to 29.6% via optimization; while after 14,000 h of operation, the difference between efficiencies is around 1.7%. Additionally, by using the determined optimal points, the average cumulative electrical efficiency is increased from 26.03% (at normal operation) to 27.56%; while applying the partialization strategy could only marginally increase this performance indicator [30].

5.4. Optimization procedure II

Optimization procedure II is carried out in order to determine the optimal operating conditions of the system while addressing a certain electrical load profile. For this purpose, the electrical generation (the demand to be addressed) and the net electrical efficiency (as an indicator of system's performance) are considered as optimization objectives. Fig. 5 depicts Pareto frontiers obtained for different intervals by applying optimization procedure II. As can be seen in this figure, the aforementioned competing relation between the objective functions (electrical efficiency and power generation) exist in all time steps. As a result, applying design parameters of optimal points with high electrical power generation leads to lower values of net electrical efficiency. On the other hand, Fig. 6 displays that through time, the Pareto frontier shifts towards regions with lower electrical efficiency and power generation which can be ascribed to the significant degradation in the fuel cell stack. As an example, the maximum achievable electrical efficiency

Table 8
Comparison between the net electrical efficiency achieved under the optimized condition (optimization procedure I), normal operation, and partialization strategy [30].

	Time step (h)						Cumulative Average (%)
	0	1000	2500	5500	10,500	14,000	
$\eta_{net,el}$ (%) – Adaptive optimization	29.6	28.8	28.4	27.7	26.8	26.1	27.56
$\eta_{net,el}$ (%) – Partialization strategy	28.9	28.1	27.4	26.5	25.6	24.7	26.26
$\eta_{net,el}$ (%) – Normal operation	28.9	28.0	27.2	26.3	25.3	24.4	26.03

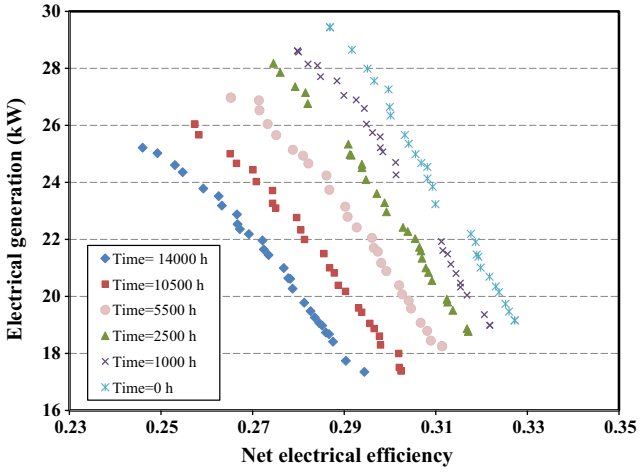

Fig. 5. Pareto front obtained from multi-objective optimization procedure II in different time steps.

of 32.72% at time zero goes down to 29.43% after 14,000 h of operation.

In order to assess the extent of performance enhancement by employing the optimal operating conditions attained from performing the optimization procedure II, the maximum electrical power obtained at different time steps are compared with those achieved under normal operation. Considering the values reported in Table 9, although the electrical power generation gradually diminishes, it can be observed that the adaptive optimization could effectively mitigate the reduction in the electrical output. As the system undergoes further degradation, the difference between the values of electrical generation under the normal condition and the optimized one becomes larger. In other words, running the plant with a single set of operating parameters for the entire lifetime increasingly distances the system from its full capacity. Using Table 9, the mentioned phenomenon can be verified by comparing the results obtained in the present study (i.e. adaptive optimization) and those borrowed from the previous work of the authors (i.e. normal operation) [30]. The difference between the generated net electrical powers under optimized condition versus normal operation starts with 1.2 kW at the beginning of operation and reaches its highest value, 1.7 kW, after 2500 h. As another performance indicator, the cumulative average power generation of the plant is also increased from 25.4 kW to 26.8 kW; the fact which verifies the considerable gain in employing the proposed adaptive optimization method to find the optimal operating parameters at each time step.

Fig. 6 presents the variation of design parameters for the optimal points (28 points) obtained from the optimization procedure II at 14,000 h (blue curve in Fig. 5). Fig. 6 reveals that for the Pareto frontier solutions anodic stoichiometric ratio and fuel aux/proc mainly fluctuate in narrow ranges (i.e. 0.148–0.165 for λ_{H_2} and 1.20–1.21 for aux/proc) while steam to carbon ratio and fuel partialization level cover a significant portion of their allowed domains. As a result, it can be deduced that running the plant by

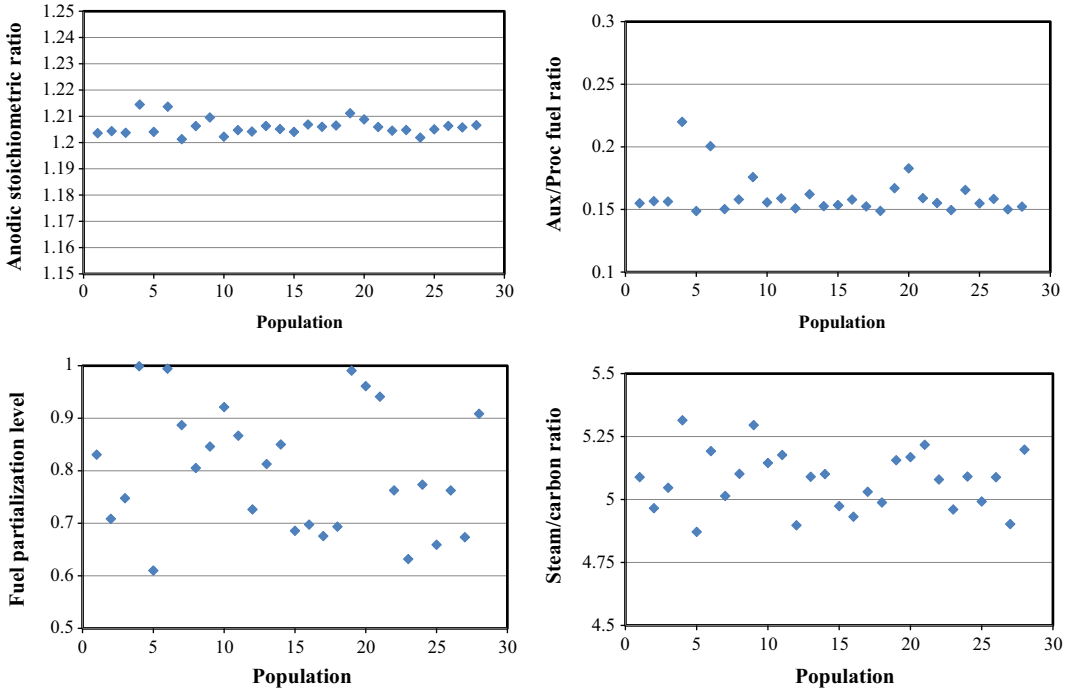

Fig. 6. Distribution of design parameters values for optimization procedure II at 14,000 h of operation.

Table 9
Comparison between the maximum electrical power generation at different time steps: using the operating conditions given by optimization procedure II and during the normal operation [30].

	Time step (h)						Cumulative average
	0	1000	2500	5500	10,500	14,000	
P_{el} (kW) – Adaptive optimization	29.4	28.6	28.2	27.0	26.0	25.2	26.8
P_{el} (kW) – Normal operation	28.2	27.3	26.5	25.6	24.7	23.8	25.4

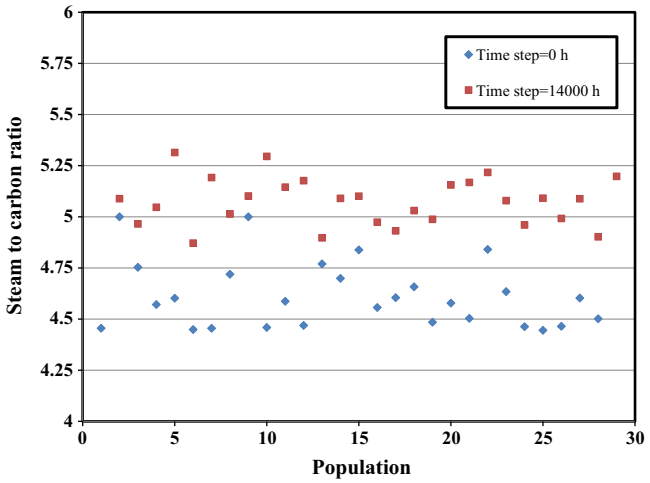

Fig. 7. Comparison between distributions of S/C for multi-objective optimization procedure II at the beginning of operation and after 14,000 h.

applying any value from the optimum ranges for λ_{H_2} and aux/proc will not significantly diminish neither of the objective functions. As can be noticed in Fig. 6, fuel partialization level sweeps its entire operating range and can be considered as the main contributor to the resulting Pareto curve. The important fact which should be underscored is the opposing impacts of fuel partialization level on the selected objective functions. On the one hand, increasing the partialization level or employing smaller values from its domain directly leads to lower electrical power generation while, on the other hand, it favors the net electrical efficiency as mentioned in the previous section (see Section 5.3).

Finally, in order to elaborate more on the importance of using adaptive optimization for a system which undergoes degradation, distributions of steam to carbon ratio for Pareto solutions at 0 h and 14,000 h (from optimization procedure II) have been reported. As can be observed in Fig. 7, optimal points at 14,000 h generally possess steam to carbon ratios greater than those at the beginning of operation. The noted upward shift in S/C values could be stemmed from the positive effect of higher S/C (in this specific range [40]) on the reforming reactions, electrical power generation, and consequently the net electrical efficiency. It is worth mentioning that even though this increment in S/C and the subsequent gain in terms of electrical power could bring about lower thermal power generation, the advantageous impact of degradation on the thermal generation hampers a sharp decline in the values of generated thermal energy.

6. Conclusion

The key purpose of the present study was to develop an effective and practical approach which enables the HT-PEM fuel cell based CHP plant to operate at maximum capacity through its lifetime. To this end, an adaptive multi-objective optimization method has been applied while considering the degradation in the fuel cell stack and the fuel processor for the first 15,000 h of operation of the system. Two different sets of objective functions have been considered: (I) net electrical efficiency and thermal generation; and (II) net electrical efficiency and electrical generation. In order to address thermal and electrical profiles, optimization procedure I and II can be implemented respectively. Steam to carbon ratio, auxiliary to process fuel ratio, fuel partialization level and anodic stoichiometric ratio were the design parameters. In both optimization methods, for each time interval, the result of optimization is a Pareto frontier which is a set of optimal points each of which has its own unique operating parameters.

Given the inevitable degradation within the components of the system, this approach can be used as a helpful tool to optimize the performance of CHP systems. Based on the desired thermal and electrical outputs, in each time interval, user can alter the operating parameters (mainly fuel partialization level and steam to carbon ration) according to the provided optimal values. In this way, the operating conditions of the system are progressively modified in an optimal way, resulting in a notable suppression of degradation effects and a significant increment in the long-term performance of the plant. Furthermore, employing the obtained optimal operating points, a stable thermal generation profile can be obtained while the performance of the unit is also improved.

Considering the optimization procedure I, in all time steps, the plant is able to cater a wide range of thermal power while, thanks to optimization, the net electrical efficiency is kept at its maximum possible value. The highest values of net electrical efficiency at time zero and after 14,000 h of operation are 32.75% and 29.51% respectively, which illustrates the significant degradation within the stack. Furthermore, it was determined that by using the optimal points, the average cumulative electrical efficiency is increased from 26.03% (at normal operation) to 27.56%; while applying the partialization strategy (suggested in our previous work) could slightly increase the efficiency.

Regarding the optimization procedure II, through time, the Pareto frontier has a noticeable shift towards regions with lower electrical efficiency and power generation. For instance, the maximum achievable electrical efficiency of 32.72% at time zero goes down to 29.43% after 14,000 h of operation. Moreover, comparing the results from this study and those extracted from the previous work of the authors (i.e. normal operation) shows the cumulative average power generation of the plant increased from 25.4 kW at normal operation to 26.8 kW at optimized condition.

Acknowledgment

This work was carried out in the framework of the project Microgen30 (EE01_00013) funded by Italian Ministry of Economic Development with the program Industria2015. The authors would also like to acknowledge ICI Caldaie S.p.A for providing technical support for this project.

References

[1] Bazyari A, Khodadadi AA, Haghighat Mamaghani A, Beheshtian J, Thompson LT, Mortazavi Y. Microporous titania–silica nanocomposite catalyst-adsorbent for ultra-deep oxidative desulfurization. Appl Catal B 2016;180:65–77.

[2] Mamaghani AH, Escandon SAA, Najafi B, Shirazi A, Rinaldi F. Techno-economic feasibility of photovoltaic, wind, diesel and hybrid electrification systems for off-grid rural electrification in Colombia. Renew Energy 2016;97:293–305.

[3] Adam A, Fraga ES, Brett DJL. Options for residential building services design using fuel cell based micro-CHP and the potential for heat integration. Appl Energy 2015;138:685–94.

[4] Staffell I, Green R. The cost of domestic fuel cell micro-CHP systems. Int J Hydrogen Energy 2013;38:1088–102.

[5] Najafi B, De Antonellis S, Intini M, Zago M, Rinaldi F, Casalegno A. A tri-generation system based on polymer electrolyte fuel cell and desiccant wheel–Part A: fuel cell system modelling and partial load analysis. Energy Convers Manage 2015;106:1450–9.

[6] Mamaghani AH, Najafi B, Casalegno A, Rinaldi F. Long-term economic analysis and optimization of an HT-PEM fuel cell based micro combined heat and power plant. Appl Therm Eng 2016.

[7] Mamaghani AH, Najafi B, Shirazi A, Rinaldi F. Exergetic, economic, and environmental evaluations and multi-objective optimization of a combined molten carbonate fuel cell-gas turbine system. Appl Therm Eng 2015;77:1–11.

[8] Guizzi GL, Manno M. Fuel cell-based cogeneration system covering data centers' energy needs. Energy 2012;41:56–64.

[9] Jannelli E, Minutillo M, Perna A. Analyzing microcogeneration systems based on LT-PEMFC and HT-PEMFC by energy balances. Appl Energy 2013;108:82–91.

[10] Zuliani N, Taccani R. Microcogeneration system based on HTPEM fuel cell fueled with natural gas: performance analysis. Appl Energy 2012;97:802–8.

[11] Kang K, Yoo H, Han D, Jo A, Lee J, Ju H. Modeling and simulations of fuel cell systems for combined heat and power generation. Int J Hydrogen Energy 2015.

[12] Napoli R, Gandiglio M, Lanzini A, Santarelli M. Techno-economic analysis of PEMFC and SOFC micro-CHP fuel cell systems for the residential sector. Energy Build 2015;103:131–46.

[13] Colella WG, Pilli SP. Energy system and thermoeconomic analysis of combined heat and power high temperature proton exchange membrane fuel cell systems for light commercial buildings. J Fuel Cell Sci Technol 2015;12.

[14] Herdem MS, Farhad S, Hamdullahpur F. Modeling and parametric study of a methanol reformate gas-fueled HT-PEMFC system for portable power generation applications. Energy Convers Manage 2015;101:19–29.

[15] Mamaghani AH, Najafi B, Shirazi A, Rinaldi F. 4E analysis and multi-objective optimization of an integrated MCFC (molten carbonate fuel cell) and ORC (organic Rankine cycle) system. Energy 2015;82:650–63.

[16] Perna A, Minutillo M, Jannelli E. Investigations on an advanced power system based on a high temperature polymer electrolyte membrane fuel cell and an organic Rankine cycle for heating and power production. Energy 2015;88:874–84.

[17] Wu Q, Li H, Yuan W, Luo Z, Wang F, Sun H, et al. Performance evaluation of an air-breathing high-temperature proton exchange membrane fuel cell. Appl Energy 2015;160:146–52.

[18] Pohl E, Maximini M, Bauschulte A, Vom Schloß J, Hermanns RTE. Degradation modeling of high temperature proton exchange membrane fuel cells using dual time scale simulation. J Power Sources 2014;275:777–84.

[19] Zhang C, Zhou W, Ehteshami MM, Wang Y, Chan SH. Determination of the optimal operating temperature range for high temperature PEM fuel cell considering its performance, CO tolerance and degradation. Energy Convers Manage 2015;105:433–41.

[20] Kim M, Kang T, Kim J, Sohn Y-J. One-dimensional modeling and analysis for performance degradation of high temperature proton exchange membrane fuel cell using PA doped PBI membrane. Solid State Ionics 2014;262:319–23.

[21] Galbiati S, Baricci A, Casalegno A, Marchesi R. Degradation in phosphoric acid doped polymer fuel cells: A 6000 h parametric investigation. Int J Hydrogen Energy 2013;38:6469–80.

[22] Moçotéguy P, Ludwig B, Scholta J, Barrera R, Ginocchio S. Long term testing in continuous mode of HT-PEMFC based H_3PO_4/PBI celtec-PMEAs for μ-CHP applications. Fuel Cells 2009;9:325–48.

[23] Hawkes A, Brett D, Brandon N. Fuel cell micro-CHP techno-economics: part 2–Model application to consider the economic and environmental impact of stack degradation. Int J Hydrogen Energy 2009;34:9558–69.

[24] Di Marcoberardino G, Roses L, Manzolini G. Technical assessment of a micro-cogeneration system based on polymer electrolyte membrane fuel cell and fluidized bed autothermal reformer. Appl Energy 2016;162:231–44.

[25] Gandiglio M, Lanzini A, Santarelli M, Leone P. Design and optimization of a proton exchange membrane fuel cell CHP system for residential use. Energy Build 2014;69:381–93.

[26] Barelli L, Bidini G, Gallorini F, Ottaviano A. An energetic–exergetic analysis of a residential CHP system based on PEM fuel cell. Appl Energy 2011;88:4334–42.

[27] Godat J, Marechal F. Optimization of a fuel cell system using process integration techniques. J Power Sources 2003;118:411–23.

[28] Arsalis A, Kær SK, Nielsen MP. Modeling and optimization of a heat-pump-assisted high temperature proton exchange membrane fuel cell micro-combined-heat-and-power system for residential applications. Appl Energy 2015;147:569–81.

[29] Xu J, Froment GF. Methane steam reforming, methanation and water-gas shift: I. Intrinsic kinetics. AIChE J 1989;35:88–96.

[30] Najafi B, Haghighat Mamaghani A, Rinaldi F, Casalegno A. Long-term performance analysis of an HT-PEM fuel cell based micro-CHP system: operational strategies. Appl Energy 2015;147:582–92.

[31] Keiski RL, Salmi T, Niemistö P, Ainassaari J, Pohjola VJ. Stationary and transient kinetics of the high temperature water-gas shift reaction. Appl Catal A 1996;137:349–70.

[32] Siegel C, Bandlamudi G, Heinzel A. Systematic characterization of a PBI/H_3PO_4 sol–gel membrane—Modeling and simulation. J Power Sources 2011;196:2735–49.

[33] Pisani L. Multi-component gas mixture diffusion through porous media: A 1D analytical solution. Int J Heat Mass Transfer 2008;51:650–60.

[34] Liu Z, Wainright JS, Litt MH, Savinell RF. Study of the oxygen reduction reaction (ORR) at Pt interfaced with phosphoric acid doped polybenzimidazole at elevated temperature and low relative humidity. Electrochim Acta 2006;51:3914–23.

[35] Baschuk JJ, Li X. Modelling CO poisoning and O_2 bleeding in a PEM fuel cell anode. Int J Energy Res 2003;27:1095–116.

[36] Bergmann A, Gerteisen D, Kurz T. Modelling of CO poisoning and its dynamics in HTPEM fuel cells. Fuel Cells 2010;10:278–87.

[37] Najafi B, Mamaghani AH, Rinaldi F, Casalegno A. Fuel partialization and power/heat shifting strategies applied to a 30 kW el high temperature PEM fuel cell based residential micro cogeneration plant. Int J Hydrogen Energy 2015;40:14224–34.

[38] Selleri T, Najafi B, Rinaldi F, Colombo G. Mathematical modeling and multi-objective optimization of a mini-channel heat exchanger via genetic algorithm. J Therm Sci Eng Appl 2013;5:031013.

[39] Najafi B, Najafi H, Idalik M. Computational fluid dynamics investigation and multi-objective optimization of an engine air-cooling system using genetic algorithm. Proc Inst Mech Eng, Part C: J Mech Eng Sci 2011;225:1389–98.

[40] Najafi B, Mamaghani AH, Baricci A, Rinaldi F, Casalegno A. Mathematical modelling and parametric study on a 30 kW el high temperature PEM fuel cell based residential micro cogeneration plant. Int J Hydrogen Energy 2015;40:1569–83.